Source parameters of moderate-to-large Chinese earthquakes from the time evolution of P-wave peak displacement on strong motion recordings

Yuan Wang [1], Simona Colombelli [2,*], Aldo Zollo [2], Jindong Song [1], Shanyou Li [1,*]

[1] Key Laboratory of Earthquake Engineering and Engineering Vibration of China Earthquake Administration, Institute of Engineering Mechanics, China Earthquake Administration

[2] Department of Physics, University of Naples Federico II

* **Corresponding author: Simona Colombelli** (simona.colombelli@unina.it), **Shanyou Li** (shanyou@iem.ac.cn)

Key Points:

- The time evolution of P-wave displacement amplitude is a proxy for the moment rate function;
- The time evolution of the P-wave amplitude carries information about source magnitude and extent;
- The earthquake rupture extent can be estimated from the analysis of the early P-wave data;

Abstract

In this work we propose and apply a straightforward methodology for the automatic characterization of the extended earthquake source, based on the progressive measurement of the P-wave displacement amplitude at the available stations deployed around the source. Specifically, we averaged the P-wave peak displacement measurements among all the available stations and corrected the observed amplitude for distance attenuation effect to build the logarithm of amplitude vs. time function, named LPDT curve. The curves have an

exponential growth shape, with an initial increase and a final plateau level. By analyzing and modelling the LPDT curves, the information about earthquake rupture process and earthquake magnitude can be obtained. We applied this method to the Chinese strong motion data from 2007-2015 with M_S ranging between 4 and 8. We used a refined model to reproduce the shape of the curves and different source models based on magnitude to infer the source-related parameters for the study dataset. Our study shows that the plateau level of LPDT curves has a clear scaling with magnitude, with no saturation effect for large events. By assuming a rupture velocity of 0.9Vs, we found a consistent self-similar, constant stress drop scaling law for earthquakes in China with stress drop mainly distributed between a lower level (0.23Mpa) and a higher level (3.74Mpa). The derived relation between the magnitude and rupture length can be used for probabilistic hazard analyses and real-time applications of Earthquake Early Warning systems.

Keywords: P-wave amplitude parameter, magnitude, rupture length, stress drop, Earthquake Early Warning

Acknowledgments:

We would like to thank the University of Naples Federico II where the work has been carried out during the visiting period. This work was supported by National Key Research and Development Program of China (2018YFC1504003). Strong motion data has been provided by China Strong-Motion Network Centre (CSMNC), China Earthquake Administration. The data will be accessible in a repository. The moment rate function of the M 8.0 Wenchuan earthquake has been provided by the USGS at the following link: https://earthquake.usgs.gov/earthquakes/eventpage/usp000g650/finite-fault.

1 Introduction

The characterization of the seismic source in terms of earthquake magnitude and source radius (or length of the rupture) is now a routinely operation in any standard seismological laboratory. However, both parameters are generally computed off-line, through fairly complex procedures, mainly performed in the frequency domain. The seismic moment, for example, is estimated from the low frequency amplitude of displacement spectra. The source radius is typically obtained from the spectral corner frequency (Brune 1970; Madariaga 1976) or from time-domain, source duration measurements, generally available several minutes after the earthquake occurrence (Boatwright 1980; Duputel et al. 2012). Although the fitting of spectral shapes is a straightforward operation, a major issue is the adequate correction of the observed spectra for path attenuation and site response effects.

With this in mind, Colombelli and Zollo (2015) looked at the time evolution of the early P-wave information and used it as a proxy for the rupture process of earthquakes to extract the seismic moment and rupture extent of moderate-to-large Japanese earthquake records. More recently, Nazeri et al. (2019) explored a similar approach using strong-motion data of the 2016-2017 Central Italy sequence and estimated moment magnitude, fault length and average stress drop for each single event. Following the idea of Colombelli and Zollo (2015) and Nazeri et al. (2019), in this study we explore a similar approach for the robust estimation of the earthquake magnitude and rupture length and applied it to a database of moderate-to-large Chinese earthquake records. The proposed method is a remarkably simple and straightforward approach to rapidly and automatically estimate two main source parameters, the earthquake magnitude and the expected length of the rupture. The methodology used in this work is also able to provide an estimation of the average stress drop ($\Delta\sigma$) for the earthquakes in our dataset.

Furthermore, the proposed methodology can be used to quickly characterize the earthquake magnitude and the expected length of the rupture, and to provide an approximate estimate of the average stress drop to be used for Earthquake Early Warning and rapid response purposes, for which accurate estimation of the rupture extend at the early stage of the process can be a useful piece of information to add to the early shake-map computation for more precise ground shaking prediction.

The aim is twofold: 1) establish source scaling relationships for moderate to large earthquakes in China and 2) build the foundation for further studying the feasibility of a network-based EEW method based on the time evolution of the early P-wave peak displacement amplitude.

2 Data and methodology

2.1 Data selection

For the present analysis, we selected the earthquakes occurred in China in the period 2007–2015. The magnitude of the events (typically, surface magnitude, M_S) varies between 4.0 and 8.0. To avoid the inclusion of bad quality data in our analysis, we selected seismic records with an epicentral distance smaller than 120 km, but for the M8 event we expanded the limit to 200 km and required that each event had at least three records. A total of 1293, 3-component accelerometric waveforms, relative to 88 earthquakes and to 540 stations was used. Two main seismic regions (Sichuan-Yunnan and Xinjiang regions) in China have been selected and Fig. 1a shows the epicentral position of the selected earthquakes and the location of stations. Fig. 1b shows the histogram distribution of the analyzed records as a function of the epicentral distance and magnitude.

2.2 P-wave peak measurements and LPDT curve

We preliminary identified the onset of the P wave on the vertical component of acceleration records, using a standard short-term/long-term average method for automatic picking (Allen, R. V., 1978). Then, we visually inspected all the available waveforms and made manual picks where necessary, to adjust potential mistakes from the automatic picking algorithm. After removing the mean value and the linear trend, the acceleration waveforms are integrated once to velocity and twice to get displacement. Finally, we applied a 0.075Hz high-pass Butterworth filter to remove the low frequency drift on displacement records. We impose the zero-crossing of the signal amplitude at the onset of the P-wave, to eliminate any potential residual noise contaminations resulting from the double integration operation.

We then measure the absolute maximum of the initial P-wave amplitude on the vertical component of displacement (named Pd) using an expanding time window, starting at the

arrival of the P-wave and moving forward with a time step of 0.01s. The peak amplitude is related to the earthquake magnitude (M) and to the source-to-receiver distance (R) through an attenuation relationship of the general form (Wu & Zhao, 2006; Zollo et al.,2006):

$$log_{10}(Pd) = A + B \cdot M + C \cdot log_{10}(R) \quad (1)$$

where Pd is the P-wave peak measurements and A, B and C are coefficients empirically determined. To estimate the coefficients of equation (1), we performed a least-squares multiple regression analysis, in which we fixed the distance attenuation coefficient (C) and chose a fixed length of the P-wave time window for the parameter measurements, which was set at 3s for $M \leq 7$ and 9s for $5.5 < M \leq 7$, respectively. Further details about the estimation of the coefficients of equation (1) are provided in Supplementary Material.

We selected 31 events with at least 10 records and magnitude ranging from 4 to 8 for the computation of the LPDT curve. For each event, the peak amplitudes Pd of all records are measured at every P-wave time window and the distance-corrected amplitudes ($logP^cd$) are obtained as $logP^cd = logPd - ClogR$.

In order to avoid the contamination of the S-waves on the selected portion of the P-wave, we picked out 4 stations with clear seismic phase randomly from the dataset in each distance bin (every 20km) and manually picked the S-wave arrival time to estimate the coefficients of the following equation:

$$Ts - Tp = b \cdot k \cdot R \quad (2)$$

where Tp is the P-wave onset time, Ts is the arrival time of the S-wave, R is the hypocentral distance in km, b = 0.13 is the coefficient derived from a linear regression analysis and k is a scale factor which was set at 0.8, to account for the uncertainty of the regression analysis. Using equation (2), as the time window increases, the stations with the expected S-wave arrivals were automatically excluded to make sure only P-wave part involved in the computation. Finally, the LPDT curve is obtained by averaging the distance-corrected amplitude of all the valid stations at each time window. The computation of the curves stops when the number of stations is less than a minimum of data (5 stations). Fig.2 shows an example of computation of the LPDT curve for the M4.6 event.

2.3 Observation and modelling of LPDT curve

As shown in Fig.2, the LPDT curve has an exponential growth shape with an initial increase, a gradual intermediate curvature and a final plateau level. Generally, the LPDT curve of larger event needs more time to reach the plateau and the plateau level of the curves scale with the final magnitude (Fig. 3a).

The shape of the LPDT curve, as obtained from the average of many stations distributed over azimuth and distance, can be interpreted as a proxy of the Moment Rate Function (MRF), from the initial time up to its maximum peak value. Therefore, two essential features of the MRF, i.e., peak value and peak time, which are both related to the source properties, should be embodied in the LPDT curves. Following the idea of Colombelli and Zollo, 2015, for near-triangular source time functions, the peak value of the MRF (related to the magnitude) will correspond to the plateau level of the LPDT curve, and the peak time of the MRF (related to rupture half-duration) is a proxy for the time at which the LPDT curve reaches its plateau level (Plateau Time). With this in mind, the magnitude and rupture duration can be estimated from the plateau level and the plateau time of the curves.

To model the LPDT curves, we fit data using the following function (Colombelli et al., 2020):

$$log_{10}P_{\mathrm{d}}(t) = P_L\left\{1-\left[ae^{-t/T1}+(1-a)\left(e^{-t/T2}\right)\right]\right\}+y_0 \qquad (3)$$

where y_0 is fixed as the first point of the curve, P_L is the interval between y_0 and the plateau level, **a** is the weighting factor which is set to 0.5, T_1 and T_2 are the time parameters (here we define the larger value as T_2). T_1 controls the very initial part which usually has a faster increasing speed and T_2 represents the second part, whose increasing speed gradually become slower. This double corner time, exponential model accounts finely for the two different behaviors of LPDT curve-that is to say, a sharp increase to the plateau (ramp-like) for small events and a more gentle and smooth increase (exponential) for largest events. The model parameters are shown in Fig. 2.

We used a non-linear, weighted-fitting approach to model our curves, accounting for the standard error on each point of LPDT curves. Specifically, at each time step, the weight is obtained as:

174 $$Weight = 1/(N \cdot SE^2) \quad (4)$$

175 where SE is the standard error in each P-wave time window, N is the number of stations used
176 for that time window. Fig. 3b shows that the LPDT (displacement) curves of all the events are
177 quite well reproduced by the fitting model, with an average residual of 0.3. Generally, at the
178 beginning of the curve computation, several stations from a broad range of distances and
179 azimuths are involved in the calculation, so that the scatter of data is large and the fitting
180 procedure gives a smaller weight to this part, as compared to the plateau of the curves, which
181 is instead, well reproduced. A slightly larger (about 0.7) difference between the real data and
182 the model is observed for the initial part of the curve of the M 8.0 Wenchuan earthquake,
183 which could be related to the complexity of the source process of this peculiar event. Indeed,
184 when looking at the seismic moment release of this event (Fig. 4), a small peak value is
185 observed at 4-5 seconds, before the arrival of the absolute main peak value (at about 25s), and
186 this leads to a sag of the LPDT curve around 4s.
187
188 **3 Results**
189 We fit the LPDT curves with our exponential model and obtain the three relevant
190 parameters mentioned above (T_1, T_2, P_L) while y_0 has been fixed to the first point amplitude.
191 For simplicity, we defined a new variable called $P_L^* = P_L + y_0$ to represent the true plateau
192 level of the LPDT curves. Both the amplitude parameter (P_L^*) and the two characteristic
193 times (T_1 and T_2) scale with earthquake magnitude. Fig. 5 shows the plateau level P_L^* as a
194 function of magnitude. A good correlation between P_L^* and magnitude (the correlation
195 coefficient reaches 0.947) can be found. The parameters T_1 and T_2 extracted from our fitting
196 model are shown in Fig. 6 as a function of magnitude. As the best fitting line indicates, both
197 parameters linearly increase with magnitude (in logarithmic scale). Due to the very rapid
198 initial increase of the curves, T_1 and T_2 are close to each other for small events, while they
199 gradually separate when the magnitude becomes larger and the initial part of the curves
200 increases gently.
201
202 **3.1 Magnitude estimation**

Once the observed amplitude has been corrected for the distance effect, the LPDT value at each P-wave time window can be associated to a corresponding magnitude using the coefficients of equation (Table S1). Fig. 3 shows the dynamic process of estimating magnitude for the LPDT curve. The y axis on the left stands for the distance corrected Pd, and the corresponding magnitude or estimated magnitude scale is shown on the right. The predicted magnitude (Mpre) then can be estimated accurately as follows:

$$Mpre = (P_L^* - A)/B \qquad (5)$$

where P_L^* is equal to the P_L + $\mathbf{y_0}$ which we fitted from our model, A and B are the coefficients of the attenuation relationship listed in Table S1. As shown in Fig. 3, the occurrence of the plateau for large events (M > 6-7) needs more than 9 seconds after the P-wave arrival, suggesting that the typical approaches for the magnitude estimate using fixed 3-4s P-wave time windows (PTWs) would provide underestimated magnitudes for such large events. Moreover, the B coefficient (calibrated using a 3 second PTW) could not be suitable to compute the corresponding magnitude based on the P_L^* obtained in a longer time window. We therefore choose two magnitude ranges, with two different PTW lengths, to calibrate and use the optimal coefficients (Table S1) for magnitude estimation. In this way, when an event reached its plateau within 4s, we use the relation coefficients A and B for fixed 3s PTW, while we used the coefficients A and B established with a fixed 9s PTW when its LPDT curve keeps increasing after 4s.

The estimated final magnitude based on the P_L^* for the LPDT curve and obtained with the two sets of coefficients for small and large events respectively, is plotted in Fig. 7 as a function of the catalog magnitude. As it can be seen in Fig. 7, most of the points are distributed around the dashed line representing the 1:1 relationship between the estimated magnitude and the catalog magnitude. The scatter of data is rather small, with an average estimated error of 0.229 magnitude units.

3.2 Prediction of rupture length and estimation of stress drop $\Delta\sigma$

The rupture duration is the total duration of a seismic event, given by the whole time length of the moment rate function (Vallée, 2013). It is generally observed that the rupture

duration scales with magnitude and is related to the rupture length, assuming a value for the rupture velocity (Wells & Coppersmith, 1994). As the moment rate function can be simplified as a symmetric triangle (Bilek et al., 2004), the peak time of the MRF, corresponding to the plateau time (T_{PL}) of the LPDT curve, is a measure of the Half-duration of each event (Colombelli & Zollo, 2015; Nazeri et al., 2019). Having in mind the Sato & Hirasawa model (Sato & Hirasawa, 1973) here we investigate the relation between parameter T_2 of LPDT curves and T_{PL}, the time at which occurs the peak of the MRF. In the Sato & Hirasawa model, the rupture spreads radially outwards at a constant velocity with a circular fault, and stress drop ($\Delta\sigma$) and rupture velocity (Vr) are two relevant parameters controlling the earthquake rupture process. Since $\Delta\sigma$ and Vr of earthquakes can vary significantly for each event (Allmann & Shearer, 2009), we performed a set of dedicated simulations to explore stress drop values between 0.05Mpa and 20 MPa with rupture velocities between 0.5Vs and 0.9Vs, for a total of 55 combinations of the two parameters.

For each given magnitude, we fixed $\Delta\sigma$ and Vr, and generate the corresponding Sato & Hirasawa moment rate Function (SHF) by changing the polar angle of the observation point from 0^o to 90^o and computing the average SHF (an example of M5 event shown in the Fig.8a). We then compute the log of the SHF (hereinafter LSHF) to get a curve with a similar shape of our LPDT curve. Since most of the selected earthquakes in our database occurred at an average depth of about 10km, we set the Vp=6.2km/s, Vs=3.4km/s based on the velocity model for this region (Weilai Wang et al., 2014). Examples of the average SHF with fixed Vr=0.7Vs and $\Delta\sigma$=0.1MPa is shown in Fig.8, while examples with other $\Delta\sigma$ values are shown in the supplemental material. For each available couple of stress drop and rupture velocity, we used the exponential model (eq. 2) to fit the LSHF curve and extract the T_2 parameter for different magnitudes. As expected, we found that T_2 has linear relationship with T_{PL} obtained directly from the peak time of the generated SHF (in logarithmic scale) for the entire magnitude range with a small deviation when exploring the $\Delta\sigma$ and Vr, suggesting that the T_2 parameter extracted from the observed curves can be used to predict T_{PL}:

$$log_{10}(T_{PL}) = 1.111(0.051)log_{10}(T_2) + 0.542(0.030) \quad (6)$$

For the circular model with a symmetric triangular shaped MRF, the obtained T_{PL} can be

regard as the Half-Duration (HD) of the source function. After averaging the peak time of the MRF from 0^o to 90^o, we obtain the averaged half-duration related to the source radius (Aki & Richards, 2002):

$$< HD >= \frac{\int_0^{\frac{\pi}{2}} \frac{a}{V_r}(1-\frac{V_r \sin\theta}{V_p})\mathrm{d}\theta}{\frac{\pi}{2}} = \frac{a}{V_r}(1-\frac{2}{\pi}\frac{V_r}{V_p}) \qquad (7)$$

where **a** is the source radius, Vr is rupture velocity and Vp is the P-wave velocity. Given the half-duration of the source, the source radius of the analyzed events can be estimated.

Fig.9 shows the predicted source radius as a function of magnitude and its corresponding half-duration with a fixed rupture velocity of 0.9Vs. Based on the computation of stress drop ($\Delta\sigma$) for the circular model using the source radius (a) and the seismic moment (M_0) (Keilis-Borok, 1959), $\Delta\sigma = \frac{7}{16}\frac{M_0}{a^3}$, the theoretical scaling lines of the source radius as a function of M with a constant $\Delta\sigma$=0.1Mpa and 10Mpa were given in the same figure as a comparison. The predicted source radius shows a similar increasing trend with the theoretical lines, indicating that the source radius of the analyzed events has a consistent self-similar, constant stress drop scaling with magnitude. Due to this, we fit the source radius with a weight-based fitting approach (same as eq. 4, here, the SE is the standard error of the source radius computed from the predicted T_{PL} and its error obtained by the error propagation approach) to obtain the best-fit constant stress drop of 0.35Mpa. In addition, we repeated the process by setting Vr=0.7Vs and Vr=0.8Vs, and found that the mean value of $\Delta\sigma$ are 0.99Mpa and 0.57Mpa, respectively.

For a circular fault, we predict the rupture length as the twice of the predicted source radius. According to the results of LPDT curve shown in Fig.11, we obtain a rupture length of 68 km with a predicting source radius of 34 km for the M 7.0 Lushan earthquake, which agrees with the source inversion results of Zhang, et al. (2014a) (L~60km). For the M 8.0 Wenchuan earthquake, we obtained a predicted rupture length of 271km, which is slightly underestimated as compared to the estimate of Zhang, et al. (2014b) (L~300km).

The MRF of M 8.0 Wenchuan earthquake (download from USGS, shown in Fig. 4) has the major peak occurring at the beginning of the rupture and followed by a long-time duration

coda. The circular model with a triangle-shape MRF is not able to correctly reproduce this kind of source function. For large earthquakes (M>6.7), indeed, the rupture length (L) extends with magnitude, but the rupture width (W) has a nearly constant value (20km) (Cheng et al., 2019). In the situation of L>>W for large events, the Haskell model with a trapezoid-shape MRF is often used.

The far-field displacement radiated by a Haskell type fault model is equivalent to the convolution of two box-car functions of different amplitude and durations: rise time (τ) and rupture time (T_R). The resulting function has a trapezoidal shape with total duration given by the sum of $\tau + T_R$. The rupture time T_R depends on the finite length of the fault (L) and the azimuth (ϑ) between source and receiver (Haskell, 1964):

$$T_R = \frac{L}{Vr}\left(1 - \frac{Vr}{Vp}\cos\vartheta\right) \quad (8)$$

The rise time τ is independent of azimuth (Hwang et al., 2011) and can be obtained using the following relationship calibrated by Melgar and Hayes (2017) from a database of finite faults:

$$\log_{10}(\tau) = -5.323 + 0.293\log_{10}(M_0) \quad (9)$$

Fig.10 shows an example of changing the azimuth (ϑ) from 0^o to 180^o to compute the average total duration. Assuming that T_{PL} is the middle point of the average trapezoid plateau, the following relationship between L and T_{PL} can be obtained and be used for estimating rupture length of large events when assuming the Haskell model:

$$T_{PL} = \frac{1}{2}\left(\tau + \frac{L}{Vr}\left(1 - \frac{Vr}{Vp}\right)\right) \quad (10)$$

We computed the predicted rupture length for the two large events using the Haskell model. Results are included in Fig.11. As shown in Fig. 11, with the same T_{PL}, Haskell model provides a rupture length slightly larger than the results using circular model for large events. The obtained earthquake scaling relationship in this study is comparable with the magnitude-rupture scaling relation studied by Cheng et al. (2019) using 91 earthquakes in Mainland China and the empirical scaling relation for strike-slip earthquakes with M 4.8 to M 8.1 proposed by Wells & Coppersmith (1994), especially in the moderate-large magnitude range.

As for the computation of stress drop, for larger events (L>>W), we used the following formula (Madariaga, 1977):

$$\Delta\sigma = \frac{2}{\pi} \bullet \frac{M_0}{W^2 L} \quad (11)$$

where W is the rupture width, set to 20km for large events (M>6.7).

We therefore suggesting using the circular model for small-moderate events (M$\leqslant$6.7) and the Haskell model (rectangle model) for large events (M>6.7) in the estimation of rupture length. Based on the predicted source radius derived from different models, we compute the stress drop of each event shown in Fig.12. After applying the rectangle source model for larger events, we obtain the stress drop = 4.88Mpa for M 8.0 Wenchuan earthquake, which is comparable with the results of Meng et al. (2019) (3.5Mpa). However, both models in this study provides an underestimated stress drop for M 7.0 Lushan earthquake when comparing with the results (1.8Mpa) obtained by Li et al. (2017). The distribution of stress drops is shown in Fig. 12b. The values vary from 0.1Mpa to 10Mpa, and two sets of values nearly distributed with a logarithmic mean of 0.23Mpa and 3.74Mpa, respectively. All these source parameters of the analyzed events are summarized in Table 1.

4 Discussion and Conclusion

In this study, we generalized the approach proposed by Colombelli and Zollo, 2015 to estimate the source parameters of a set of Chinese earthquakes with magnitude ranging from 4 to 8. The methodology is based on the use of the time evolution of the P wave (LPDT curve) as a proxy for the source time function to extract earthquake magnitude and rupture duration.

Comparing with the previous works by Colombelli and Zollo (2015) and Nazeri et al. (2019), we used the double corner time, exponential model proposed by Colombelli et al. (2020) for better modelling the behavior of LPDT curves. We improved the magnitude estimation based on the plateau level of LPDT curve, by using two different scaling coefficients with fixed C, which have been properly calibrated. A high correlation between magnitude and plateau level has been found and was used to predict the final magnitude accurately.

This paper proposes a method to obtain a reliable magnitude estimation using a

straightforward, time-domain signal processing technique, from the plateau level of the LPDT curves are. Based on the analysis of 31 events in the magnitude range between 4 and 8, we found that the plateau level of LPDT curves has a strong correlation with magnitude (the coefficient of correlation is up to 0.947). Comparing with the catalog magnitude of the analyzed events, our predicted magnitude from the displacement data shows an average deviation of 0.229 magnitude units. Surprisingly, for the largest Wenchuan earthquake (Ms 8.0) we provide a magnitude estimation of 8.3, without saturation effects, typically observed when using shorter P-wave time windows (Lomax et al., 2009; Bormann et al., 2009; Colombelli et al., 2012).

Together with the plateau level, the plateau time (T_{PL}) of the LPDT curve has also a clear scaling with magnitude, being related to the half-duration of the source. In order to estimate the plateau time, we performed a series of simulations based on the Sato & Hirasawa (Sato & Hirasawa, 1973) model and on the assumption that T_{PL} corresponds to the peak time of the MRF. We generated a set of MRFs exploring $\Delta\sigma$ and Vr values and studied the relation between T_{PL} and the time characteristic parameter T_2. Finally, we established a linear scaling relationship between the two parameters for predicting the T_{PL}.

Considering the circular model with a symmetric triangular-shaped MRF, the obtained T_{PL} can be regarded as the Half-Duration (HD) of the events to predict the source radius. The obtained source radius in this study shows a consistent self-similar, constant stress drop scaling with magnitude. We obtained the best-fit stress drop (0.35Mpa) for the 31 analyzed events, with fixing rupture velocity to 0.9Vs. This value is lower than world-wide measured median value of 4 MPa (Allmann and Shearer, 2009), but it is comparable with the mean value of 0.52MPa by studying the strong-motion recordings of the Wenchuan aftershocks (2008-2013) (Wang et al., 2018).

One major result of this paper concerns the determination of the scaling law of earthquakes in China. We obtained the rupture length (twice source radius) of the analyzed events and found the M 8.0 Wenchuan earthquake has a slightly shorter predicted rupture length with comparing to other results. We realize that for the largest events in the sequence, the circular model may underestimate the total rupture length. Thus, we suggested to estimate the rupture length of the large events (M>6.7) assuming the Haskell model. Our predicted

rupture length of different source models as a function of M is close to the rupture scaling relationship proposed by Cheng et al. (2019) and Wells & Coppersmith (1994). It could be used for probabilistic hazard analyses, especially for moderate-large events.

To better investigate the distribution of the stress drop in the study dataset, we used the rectangular model instead of the circular model to compute the stress drop of individual earthquakes for larger events. The derived stress drop from displacement is mainly distributed at a lower level (0.23Mpa) and a higher level (3.74Mpa) close to the world-wide measured median value (4Mpa). The lower stress drop group ($\Delta\sigma$<0.6Mpa) consists of 18 events, in which half of the events are aftershock. Consistent with Wang et al. (2018), the lower stress drop of aftershocks may result from the remaining locked parts on the fault plane of the mainshock. Moreover, we notice that if there is a jump in the increasing process of the LPDT curve (e.g. M 6.6 Ludian earthquake), our approach likely fits the event with a longer T_2 causing lower stress drop.

The shape of the curves may change in real-time, when we do not have all the available stations. As a perspective of the work, we could evaluate the feasibility of application in real-time, that can be relevant for EEW applications. Thus, both estimated results can be jointly used to provide a specific early-Shakemap for EEWS. While in this off-line study we used the post-earthquake location instead of the real-time estimation, a reliable estimation of the earthquake location is needed for the real-time application. Having in mind that the far-field stations must wait enough time to reach the plateau of the curve for large events, we need more time to get the plateau information. Hence, the real-time application performance and the timeliness based on the network distribution for this approach will be further studied. A possible method could be that we can estimate the final curve at each time step with a given probability and study the real-time curve reached how many percent of the final curve (maybe after T_2) can give a reliable probability for estimating final curve.

References

Aki, K., & Richards, P. G. (2002). Quantitative seismology. Sausalito, CA: University Science Books.

Allen, R. V. (1978). Automatic earthquake recognition and timing from single traces. *Bulletin*

404 *of the Seismological Society of America, 68*(5), 1521– 1532.
405 Allmann, B. P., & Shearer, P. (2009). Global variations of stress drop for moderate to large
406 earthquakes. *Journal of Geophysical Research: Solid Earth, 114*(B1), B01310.
407 https://doi.org/10.1029/2008jb005821.
408 Bilek, S., Lay, T., & Ruff, L. (2004). Radiated seismic energy and earthquake source duration
409 variations from teleseismic source time functions for shallow subduction zone thrust
410 earthquakes. *Journal of Geophysical Research: Solid Earth, 109*(B9), B09308.
411 https://doi.org/10.1029/2004jb003039.
412 Boatwright J (1980) A spectral theory for circular seismic sources; simple estimates of source
413 dimension, dynamic stress drop, and radiated seismic energy. *Bulletin of the*
414 *Seismological Society of America 70*:1-27
415 Bormann, P., & Saul, J. (2009). Earthquake magnitude. In Meyers, R. editors, Encyclopedia
416 of Complexity and Systems Science, New York, N Y: Springer.
417 https://doi.org/10.1007/978-0-387-30440-3_151.
418 Cheng, J., Wu, Z., Liu, J., Jiang, C., Xu, X., Fang, L., et al. (2015). Preliminary Report on the
419 3 August 2014, Mw 6.2/Ms 6.5 Ludian, Yunnan-Sichuan Border, Southwest China,
420 Earthquake. *Seismological Research Letters, 86*(3), 750-763. doi:10.1785/0220140208
421 Cheng, J., Rong, Y., Magistrale, H., Chen, G., & Xu, X. (2019). Earthquake Rupture Scaling
422 Relations for Mainland China. *Seismological Research Letters, 91*(1), 248-261.
423 doi:10.1785/0220190129
424 Colombelli, S., Zollo, A., Festa, G. & Kanamori, H. (2012). Early magnitude and potential
425 damage zone estimates for the great Mw 9 Tohoku-Oki earthquake. *Geophysical*
426 *Research Letters, 39*(22), L22306. https://doi.org/10.1029/2012GL053923.
427 Colombelli, S. & Zollo, A. (2015). Fast determination of earthquake magnitude and fault
428 extent from real-time P-wave recordings. *Geophysical Journal International, 202*(2),
429 1158-1163. https://doi.org/10.1093/gji/ggv217.
430 Simona Colombelli, Gaetano Festa, Aldo Zollo, Early rupture signals predict the final
431 earthquake size, *Geophysical Journal International*, ggaa343,
432 https://doi.org/10.1093/gji/ggaa343
433 Courboulex, F., Vallée, M., Causse, M. & Chounet, A. (2016). Stress-Drop Variability of

Shallow Earthquakes Extracted from a Global Database of Source Time Functions. *Seismological Research Letters, 87*(4), 912-918. https://doi.org/10.1785/0220150283.

Duputel Z, Rivera L, Kanamori H, Hayes G (2012) W phase source inversion for moderate to large earthquakes (1990–2010) *Geophysical Journal International 189*:1125-1147 doi:10.1111/j.1365-246X.2012.05419.x

Fang, L., Wu, J., Liu, J., Cheng, J., Jiang, C., Han, L., et al. (2015). Preliminary Report on the 22 November 2014 Mw 6.1/Ms 6.3 Kangding Earthquake, Western Sichuan, China. *Seismological Research Letters, 86*(6), 1603-1613. doi:10.1785/0220150006

Haskell, N.A. (1964). Total energy and energy spectra density of elastic waves from propagating faults. *Bulletin of the Seismological Society of America, 54,* 1811-1841.

Heaton, T. (1990). Evidence for and implications of self-healing pulses of slip in earthquake rupture. *Physics of the Earth and Planetary Interiors, 64*(1), 1-20. https://doi.org/ 10.1016/0031-9201(90)90002-f.

Huang, Y., Wu, J., Zhang, T., & Zhang, D. (2008). Relocation of the M8.0 Wenchuan earthquake and its aftershock sequence. *Science in China Series D: Earth Sciences, 51*(12), 1703-1711. doi:10.1007/s11430-008-0135-z

Hwang, R.-D., Chang, J.-P., Wang, C.-Y., Wu, J.-J., Kuo, C.-H., Tsai, Y.-W., et al. (2011). Rise time and source duration of the 2008 MW 7.9 Wenchuan (China) earthquake as revealed by Rayleigh waves. *Earth, Planets and Space, 63*(5), 427-434. doi:10.5047/eps.2011.01.002

Jiang, G., Wen, Y., Liu, Y., Xu, X., Fang, L., Chen, G., et al. (2015). Joint analysis of the 2014 Kangding, southwest China, earthquake sequence with seismicity relocation and InSAR inversion. *Geophysical Research Letters, 42*(9), 3273-3281. doi:10.1002/2015gl063750

Keilis-Borok, V. I. (1959), On estimation of the displacement in an earthquake source and of source dimensions, *Ann. Geofis. (Rome), 12,* 205-214. https://doi.org/10.4401/ag-5718.

Li, J., Liu, C.-L., Zheng Y., & Xiong X. (2017). Rupture process of the Ms 7.0 Lushan earthquake determined by joint inversion of local static GPS records, strong motion data, and teleseismograms. *Journal of Earth Science, 28*(2), 404-410. doi:10.1007/s12583-017-0757-1

Lomax, A., & Michelini, A. (2009). Mwpd: A duration-amplitude procedure for rapid

464 determination of earthquake magnitude and tsunamigenic potential from P waveforms.
465 *Geophysical Journal International*, *176*(1), 200–214.
466 https://doi.org/10.1111/j.1365-246x.2008.03974.x.
467 Madariaga R (1976) Dynamics of an expanding circular fault. *Bulletin of the Seismological*
468 *Society of America* 66:639-666
469 Madariaga. (1977). Implications of Stress-Drop Models of Earthquakes for the Inversion of
470 Stress Drop from Seismic Observations. *Pure and Applied Geophysics*, *115*, 301-316,
471 1977.
472 Meng, L., Zang, Y., McGarr, A., & Zhou, L. (2019). High-Frequency Ground Motion and
473 Source Characteristics of the 2008 Wenchuan and 2013 Lushan, China, Earthquakes.
474 *Pure and Applied Geophysics, 177*(1), 81-93. doi:10.1007/s00024-019-02291-4
475 Melgar, D., & Hayes, G. P. (2017). Systematic Observations of the Slip Pulse Properties of
476 Large Earthquake Ruptures. *Geophysical Research Letters*, *44*(19), 9691-9698.
477 doi:10.1002/2017gl074916
478 Nazeri, S., Colombelli, S., & Zollo, A. (2019). Fast and accurate determination of earthquake
479 moment, rupture length and stress release for the 2016–2017 Central Italy seismic
480 sequence. *Geophysical Journal International*, *217*(2), 1425-1432.
481 https://doi.org/10.1093/gji/ggz097.
482 SATO, T., & HIRASAWA, T. (1973). Body wave spectra from propagating shear cracks.
483 *Journal of Physics of the Earth*, *21*(4), 415-431. https://doi.org/10.4294/jpe1952.21.415.
484 Vallée, M. (2013). Source time function properties indicate a strain drop independent of
485 earthquake depth and magnitude. *Nature Communications*, 4, 2606.
486 https://doi.org/10.1038/ncomms3606.
487 Wang, H., Ren, Y., & Wen, R. (2018). Source parameters, path attenuation and site effects
488 from strong-motion recordings of the Wenchuan aftershocks (2008–2013) using a
489 non-parametric generalized inversion technique. *Geophysical Journal International*,
490 *212*(2), 872-890. doi:10.1093/gji/ggx447
491 Wang, W., Wu, J., Fang, L., Lai, G., Yang, T., & Cai, Y. (2014). S wave velocity structure in
492 southwest China from surface wave tomography and receiver functions. *Journal of*
493 *Geophysical Research: Solid Earth*, *119*(2), 1061-1078.

https://doi.org/10.1002/2013JB010317.

Wells, D. L., & Coppersmith, K. J. (1994). New Empirical Relationships among Magnitude, Rupture Length, Rupture Width, Rupture Area, and Surface Displacement. *Bulletin of the Seismological Society of America*, *84*(4), 974-1002. https://doi.org/10.1007/BF00808290.

Zhang, Y., Wang, R., Chen, Y. t., Xu, L., Du, F., Jin, M., et al. (2014a). Kinematic Rupture Model and Hypocenter Relocation of the 2013 Mw 6.6 Lushan Earthquake Constrained by Strong-Motion and Teleseismic Data. *Seismological Research Letters, 85*(1), 15-22. doi:10.1785/0220130126

Zhang, Y., Wang, R., Zschau, J., Chen, Y.-t., Parolai, S., & Dahm, T. (2014b). Automatic imaging of earthquake rupture processes by iterative deconvolution and stacking of high-rate GPS and strong motion seismograms. *Journal of Geophysical Research: Solid Earth, 119*(7), 5633-5650. doi:10.1002/2013jb010469

Zollo, A., Lancieri, M., and Nielsen, S. (2006), Earthquake magnitude estimation from peak amplitudes of very early seismic signals on strong motion records, *Geophysical Research Letters, 33*, L23312, doi:10.1029/2006GL027795

.

512 **Figures**

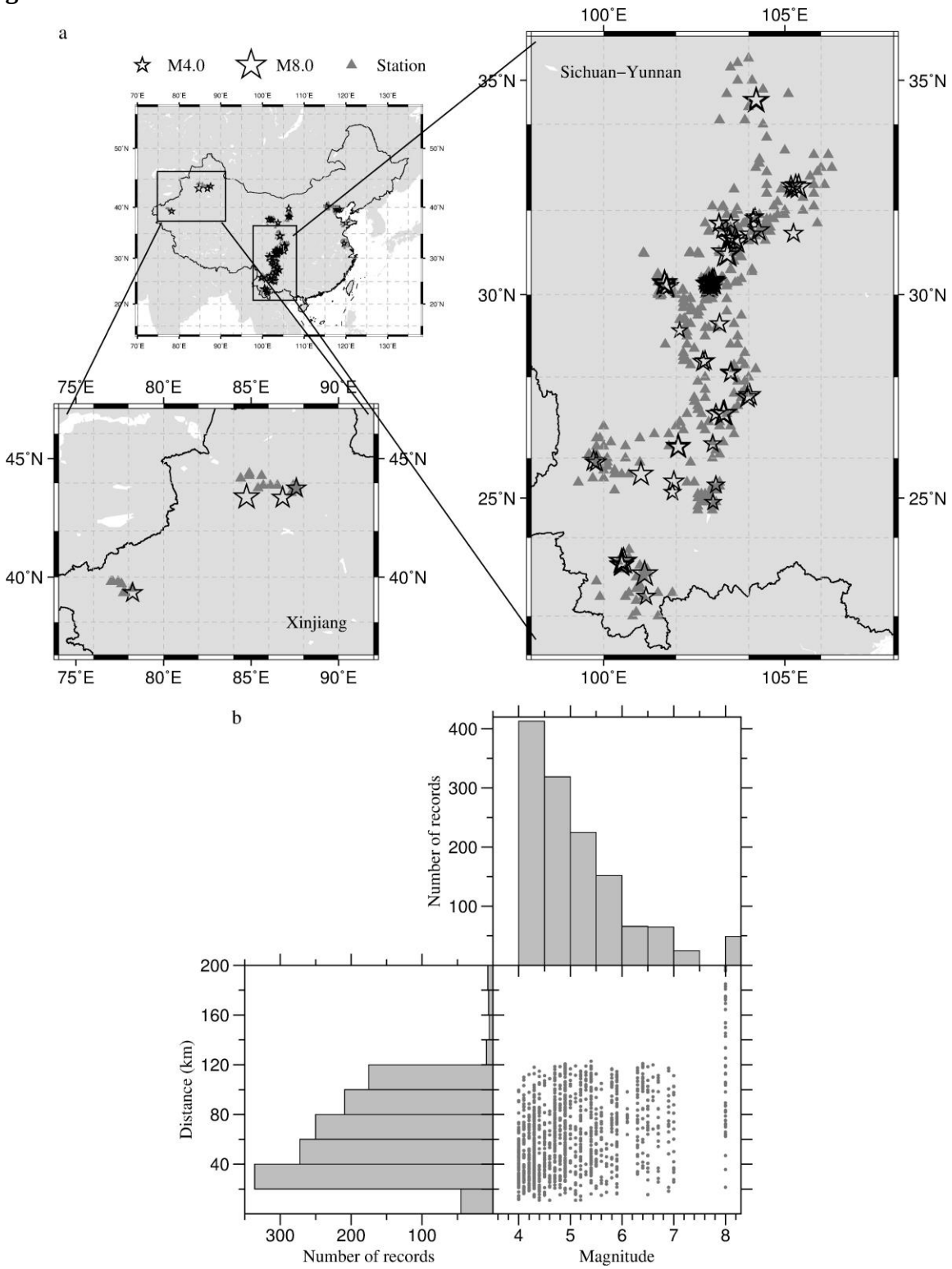

Fig.1 Data distribution. Plot of (a) the epicentral position of the selected earthquakes and the location of stations and (b) the distribution of the analyzed records as a function of the epicentral distance and magnitude.

513

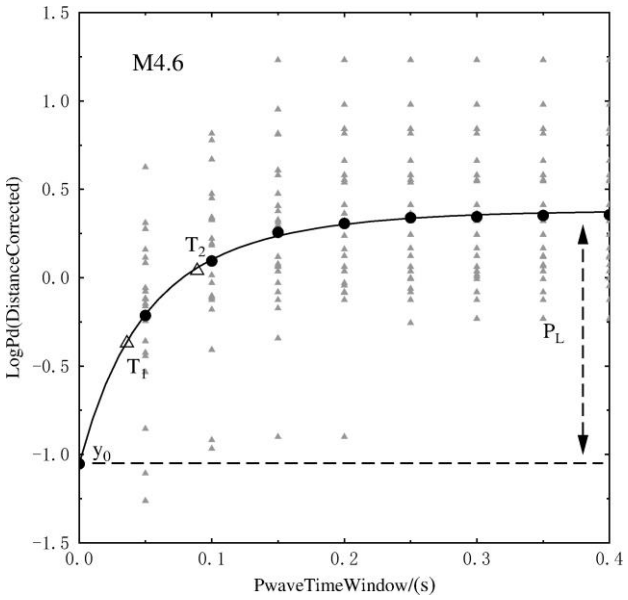

Fig.2 The LPDT curve of M4.6 event and the model parameters. The grey triangles stand for the corrected amplitude Pd^C for the available stations at each P-wave time window, then the circle represents the average Pd^C value of all these stations. Our exponential fit model is shown in black line. The time parameters T_1 and T_2 are shown in the empty triangles.

514

515

516

517

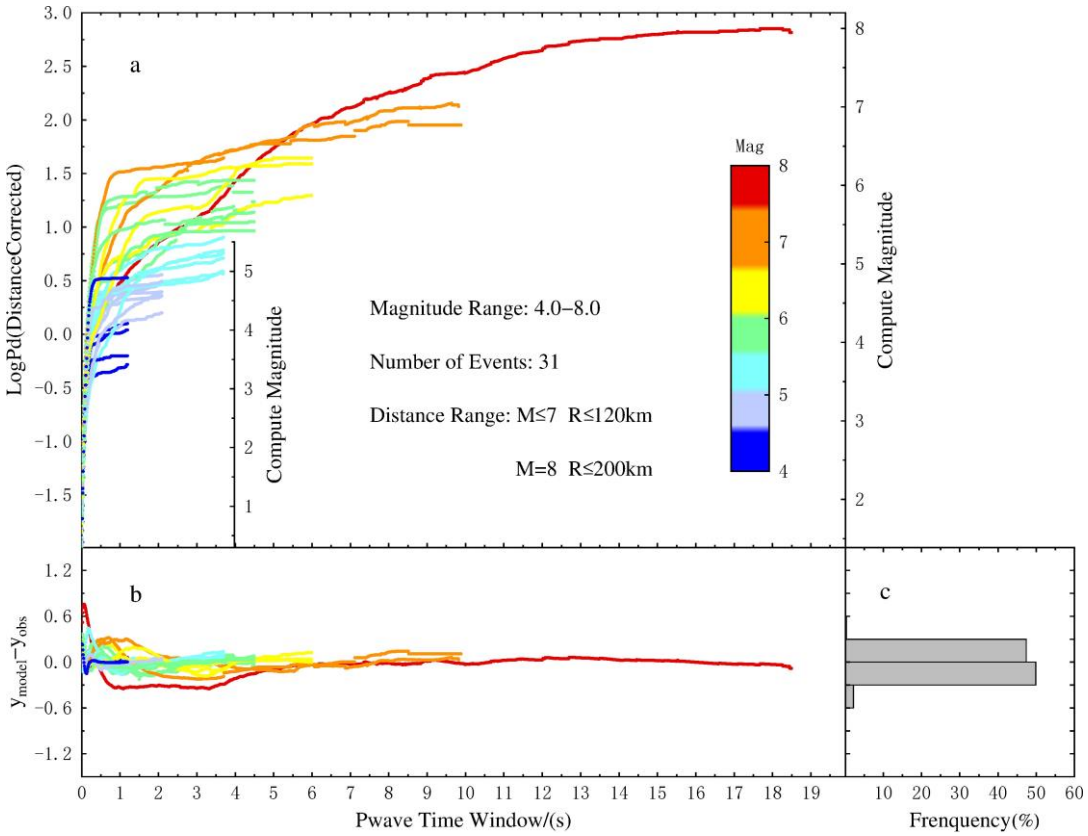

Fig.3 The LPDT curve and the misfit. (a) The average peak amplitude with distance corrected at each P-wave time window for different magnitude with color scale. (b) The difference between the observed value and the value form the fit model. (c) The normalized histograms of the misfit value.

518

519

520

521

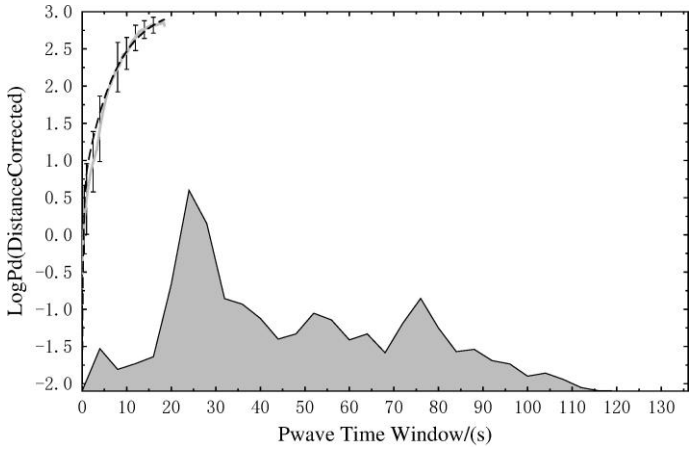

Fig.4 The LPDT curve of the M 8.0 Wenchuan earthquake and its fit model. The grey and the dashed line represent the observed data and the best fit model, respectively. The moment rate function of this event provided by the USGS was shown in the bottom with grey area.

522

523

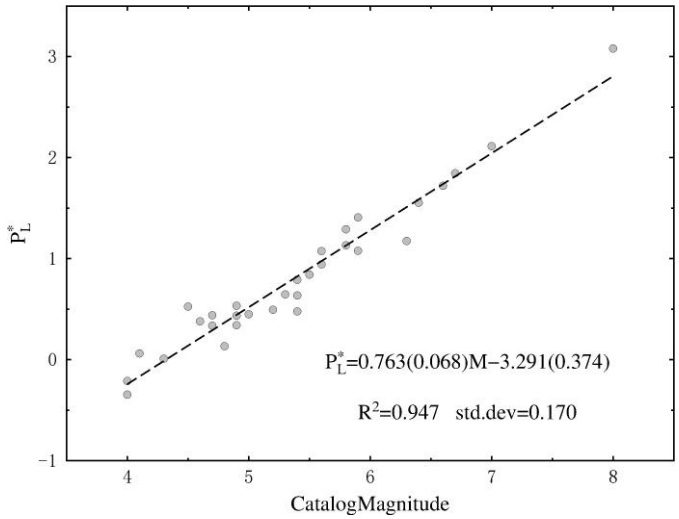

Fig.5 Scaling relationship between P_L* and magnitude. The circles present the P_L* value of each event. The dashed line indicates the best-fit relation between P_L* and magnitude.

524

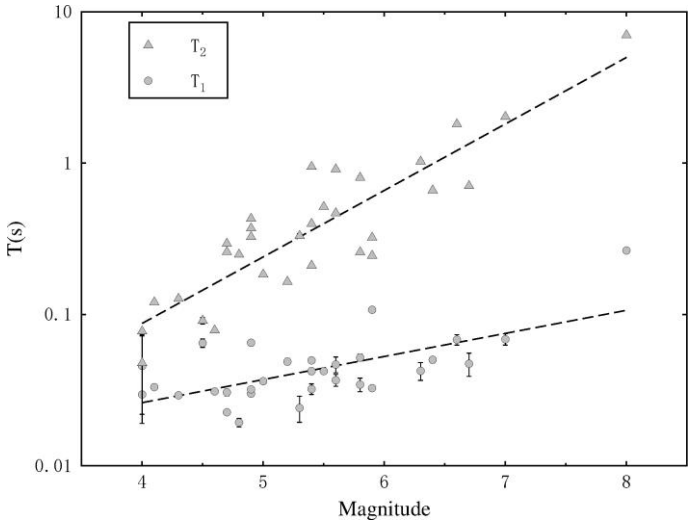

Fig.6 Scaling relationship between T1 and T2 as a function of magnitude. Triangles and circles represent T2 and T1, respectively, for both LPDT, LPVT and LPAT curves. The error bar on each single point is shown as black line (where visible). The best fitting line for each parameter is shown as dashed line.

525

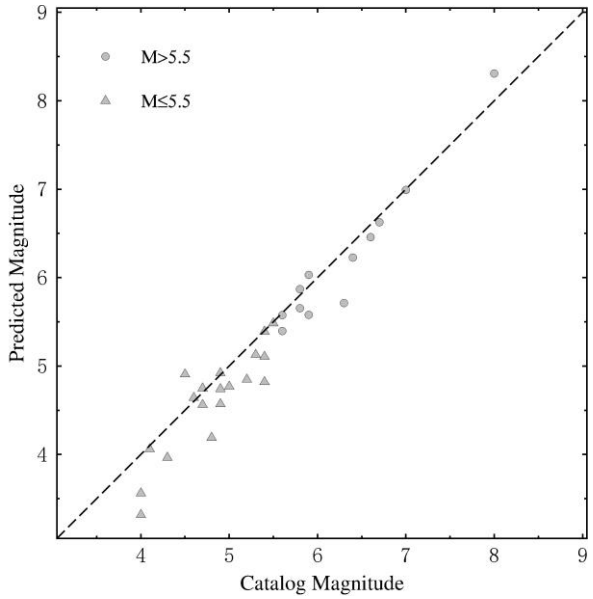

Fig.7 The estimation of the magnitude and catalog magnitude. Dashed line represents the 1:1 relationship between the estimated magnitude with PL* and the catalog magnitude.

526

527

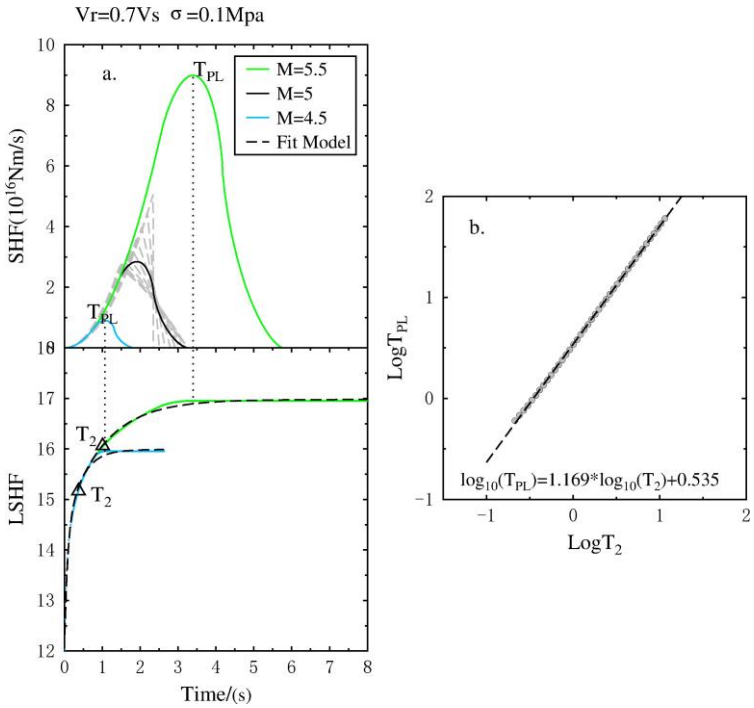

Fig.8 The exploratory simulations for Δσ = 0.1Mpa. (a) Fitting of the Sato & Hirasawa function with exponential model. The dashed line represents the fitted model. (b) Relationship between T_2 and T_{PL} for magnitude from 4 to 8 with an interval of 0.1 magnitude units. The dashed line shows the fitting relationship between T_2 and T_{PL}.

528

529

530

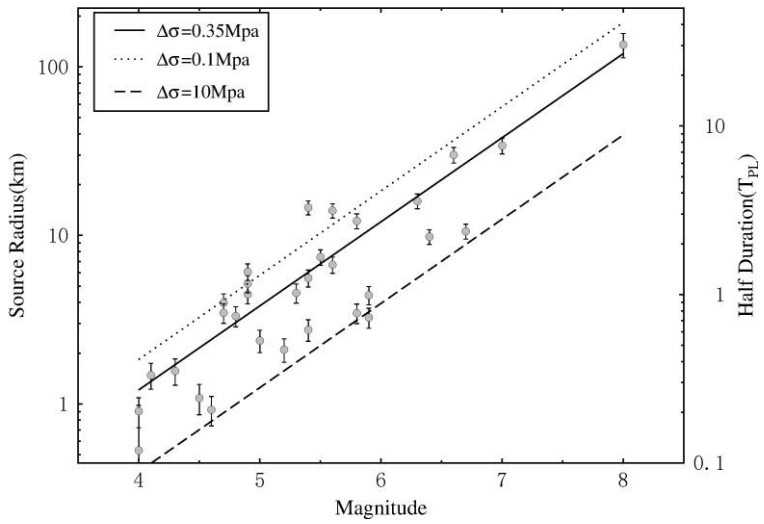

Fig.9 The scaling relation between source radius and magnitude with a fixed rupture velocity of 0.9Vs. The right y-axis represents the corresponding Half-duration. The circles stand for the T_{PL} parameter extracted from LPDT curve. The dotted line and dashed line represent the theoretical scaling with constant $\Delta\sigma$=0.1Mpa and 10Mpa, respectively. The averaged constant $\Delta\sigma$ of the analyzed dataset are shown in the solid line.

531

532

533

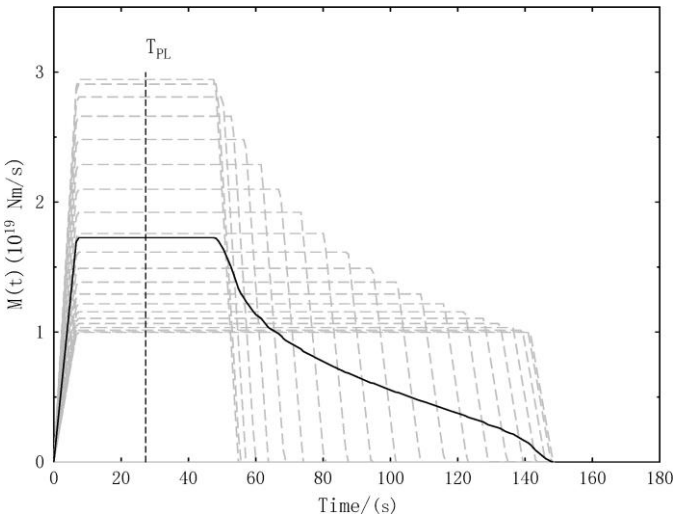

Fig.10 The trapezoid-like moment rate function (MRF) and the averaged MRF with azimuth from 0^o to 180^o. The dashed black line represents that the T_{PL} of the LPDT curves (Plateau time) occurs at the middle point of the average trapezoid plateau.

534

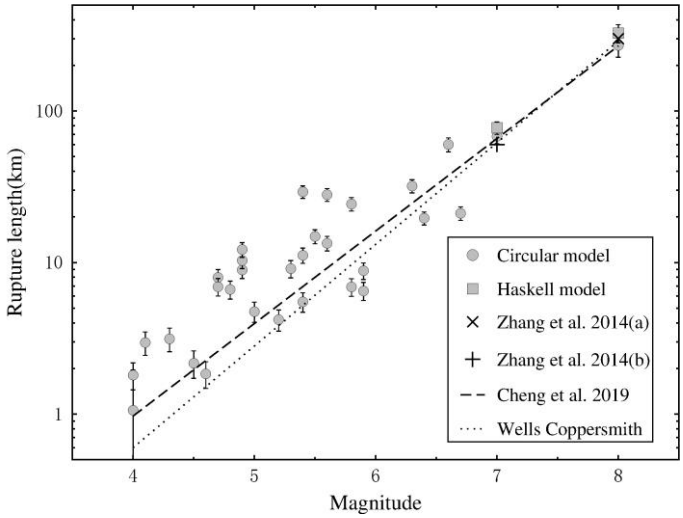

Fig.11 The scaling relationship between the predicted rupture length and M. The circles and the squares are the predicted rupture length from circular model and Haskell model, respectively. The dashed line is the linear regression relationship in mainland China calibrated by Cheng et al. (2019). The dotted line represents the relationship proposed by Wells and Coppersmith (1994). The diagonal cross and cross are the results of M 8.0 Wenchuan earthquake by Zhang et al. (2014a) and M 7.0 Lushan earthquake by Zhang et al. (2014b), respectively. The estimated error computed through the error propagation approach was shown by the vertical error bars.

535

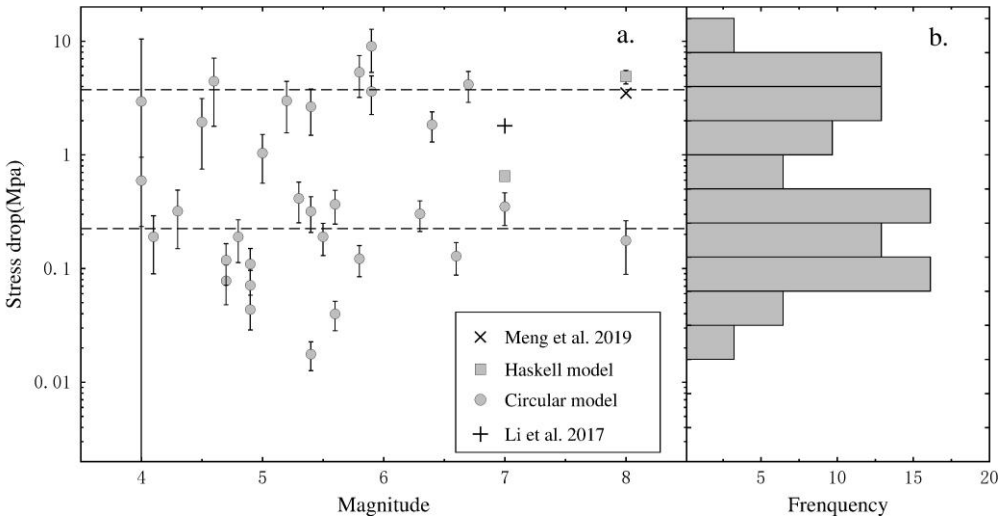

Fig.12 The estimated stress drop of the analyzed earthquakes. (a) The distribution of the estimated stress drop. The circles and the squares are the predicted stress drop from circular model and Haskell model, respectively. The average stress drop value (0.23 MPa and 3.74Mpa) is shown as a dashed line. The diagonal cross and cross are the results of M 8.0 Wenchuan earthquake by Meng et al. (2019) and M 7.0 Lushan earthquake by Li et al. (2017), respectively. (b) The normalized histograms of the predicted stress drop.

536

537

Table 1. List of source parameters including catalog magnitude (Ms), predicted magnitude (Ms^{PRED}), half duration, source radius (SR), Rupture length (RL) and stress drop ($\Delta\sigma$) determined in this study for moderate-larger events ($M \geqslant 5.5$).

No.	Location	Date	Epicenter		Magnitude			Half duration		Rupture parameters				Reference
			Lat.	Long.	M_S	M_S^{PRED}	M_W (source)	LPDT	GCMT	*SR (km)*	*RL (km)*	*RL (WC94)*	*SSD (Mpa)*	
1	Wenchuan	2008/05/12	31.00	103.40	8.0	8.3	7.9 (GCMT)	30.4	21.8	135.5	271 (circular)	248	0.18	This study
											326 (Haskell)		4.9	
											300			Zhang, Wang, Zschau, et al. (2014)
													3.5	Meng et al., (2019)
2	Wenchuan (aftershock)	2008/05/13	31.43	104.06	5.8	5.9	5.6 (GCMT)	0.8	1.6	3.4	6.8	7.1	5.34	This study
										4.3			0.73	Wang et al. (2017)
3	Wenchuan (aftershock)	2008/05/14	31.34	103.63	5.8	5.7	5.4 (GCMT)	2.7	1.3	12.2	24.4	5.2	0.12	This study
										7.5			0.17	Wang et al. (2017)
4	Yaoan	2009/07/09	25.60	101.03	6.3	5.7	5.7 (GCMT)	3.6	1.8	16.0	32	8.3	0.30	This study
5	Yiliang	2012/09/07	27.56	104.03	5.6	5.6	5.3 (GCMT)	3.1	1.1	14	28	4.5	0.04	This study
6	Eryuan	2013/03/03	25.93	99.72	5.5	5.3	5.4 (GCMT)	1.7	1.2	7.4	14.8	5.2	0.19	This study
7	Changji	2013/03/29	43.40	86.80	5.6	5.4	5.4 (GCMT)	1.5	1.3	6.7	13.4	5.2	0.37	This study
8	Lushan	2013/04/20	30.30	103.00	7	7.0	6.6 (GCMT)	7.6	4.9	34	68 (circular)	33.4	0.35	This study
											77.3 (Haskell)		0.65	
											60			Zhang, Wang, Chen, et al. (2014)
													1.8	Li et al., (2017)
9	Minxian	2013/07/22	34.54	104.21	6.7	6.6	6.0 (GCMT)	2.4	2.4	10.6	21.2	13.2	4.16	This study

10	Ludian	2014/08/03	27.11	103.33	6.6	6.5	6.2 (GCMT)	6.7	2.9	30.0	60	18.0	0.13	This study
											12			Cheng et al., (2015)
11	Kangding	2014/11/22	30.29	101.68	6.4	6.2	6.1 (GCMT)	2.2	2.8	9.8	19.6	15.4	1.85	This study
											20			Fang et al., (2015)
											16			Jiang et al., (2015)
12	Kangding	2014/11/25	30.20	101.75	5.9	5.6	5.7 (GCMT)	0.73	1.8	3.2	6.4	8.3	9.03	This study
13	Jinggu	2014/12/06	23.32	100.50	5.9	6.0	5.5 (GCMT)	1.0	1.5	4.4	8.8	6.1	3.61	This study

M_S^{PRED} = Predicted Ms, SR = source radius, RL = rupture length =2*source radius, WC94 = Wells and Coppersmith (1994), SSD = statics stress drop,

GCMT data are available at www.globalcmt.org (last accessed May.6, 2020)

538

539

Supplementary Material

Text S1. Coefficients of amplitude parameters attenuation relationship

We first use the least squared multiple regression to fit the data and found the coefficients in a fixed 3s time window. However, this time window is not enough to properly describe the amplitude for the far-field waveform of the large events. Then, we tried to apply the changed coefficients at each time window, but the changed coefficient C will induce the step change and discontinuity of the LPDT curve. Considering that coefficient C is critical in correcting distance attenuation and is closely connected with the shape of the LPDT curve, we determine the C value for each P-wave peak measurements first, and then selecting records that only P-wave included at each corresponding time window length with following selection and the relationships will be calibrated by using fixed C value. Coefficients of attenuation relationship for a short fixed 3s PTW and a long fixed 9s PTW were listed in Table S1.

.

Table S1. Coefficients of equation (1) for each magnitude range in different PTW

Coefficient	M≤7 & Fixed 3s PTW	5.5<M≤7 & Fixed 9s PTW
A	-2.16±0.13	-3.02±0.69
B	0.54±0.02	0.73±0.11
C	-1.59	

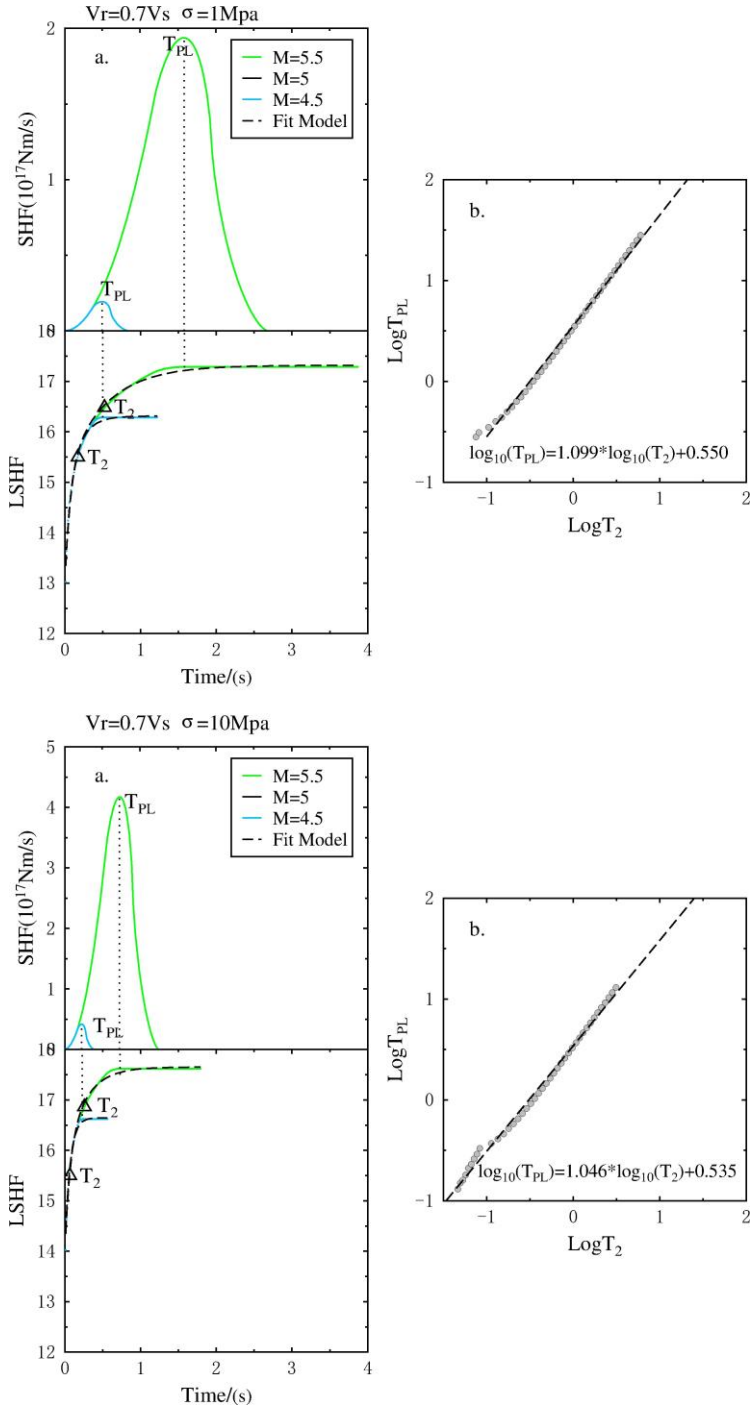

557

558 **Figure S1. The exploratory simulations for $\Delta\sigma$ = 1 and 10 Mpa.** (a) Fitting of the Sato &
559 Hirasawa function with exponential model. The dashed line represents the fitted model. (b)
560 Relationship between T_2 and T_{PL} for magnitude from 4 to 8 with an interval of 0.1 magnitude
561 units. The dashed line shows the fitting relationship between T_2 and T_{PL}.

Figure 1.

a

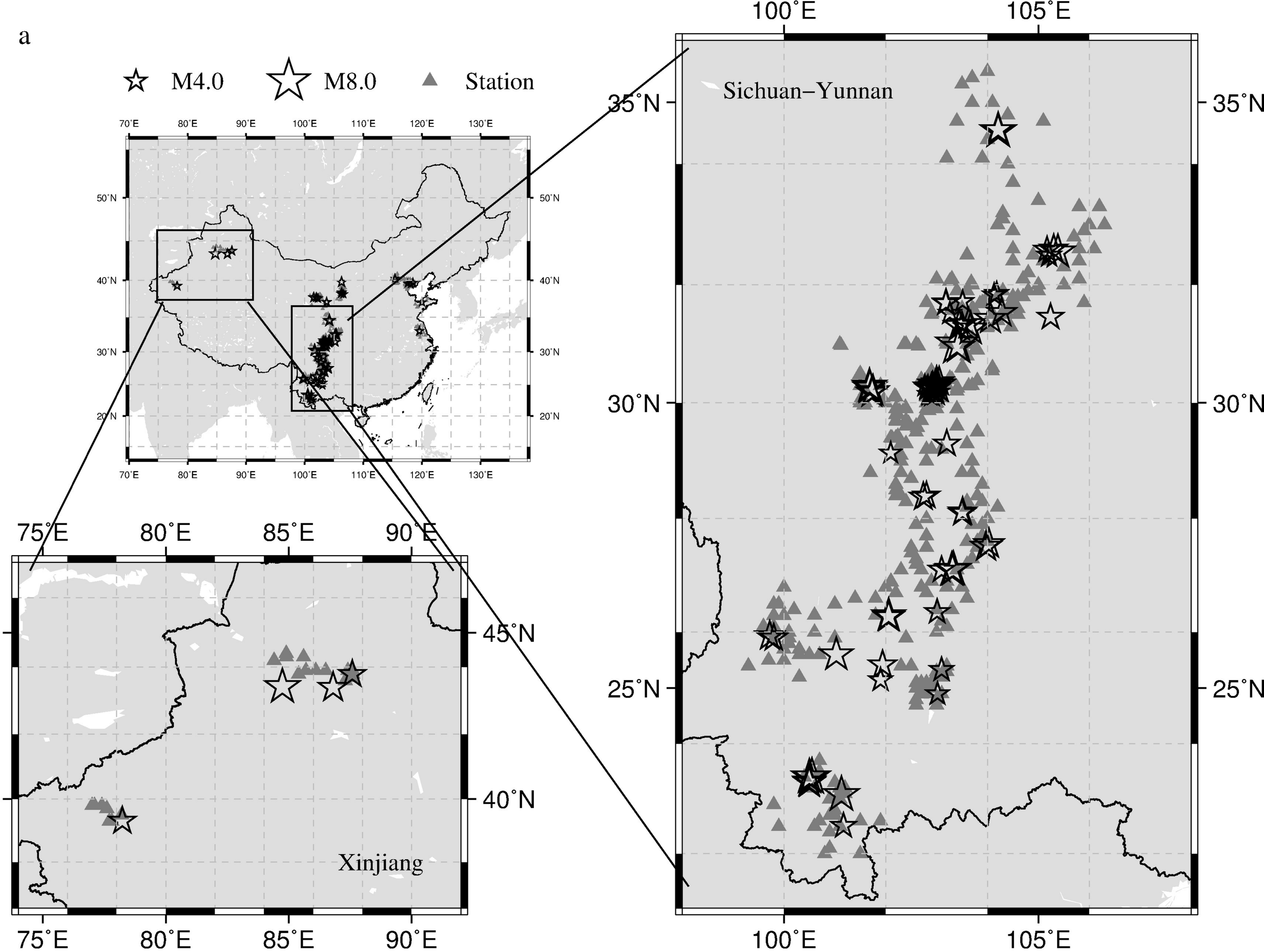
M4.0
M8.0
Station
70°E
80°E
90°E
100°E
110°E
120°E
130°E
50°N
40°N
30°N
20°N
75°E
85°E
45°N
Xinjiang
105°E
35°N
25°N
Sichuan−Yunnan

b

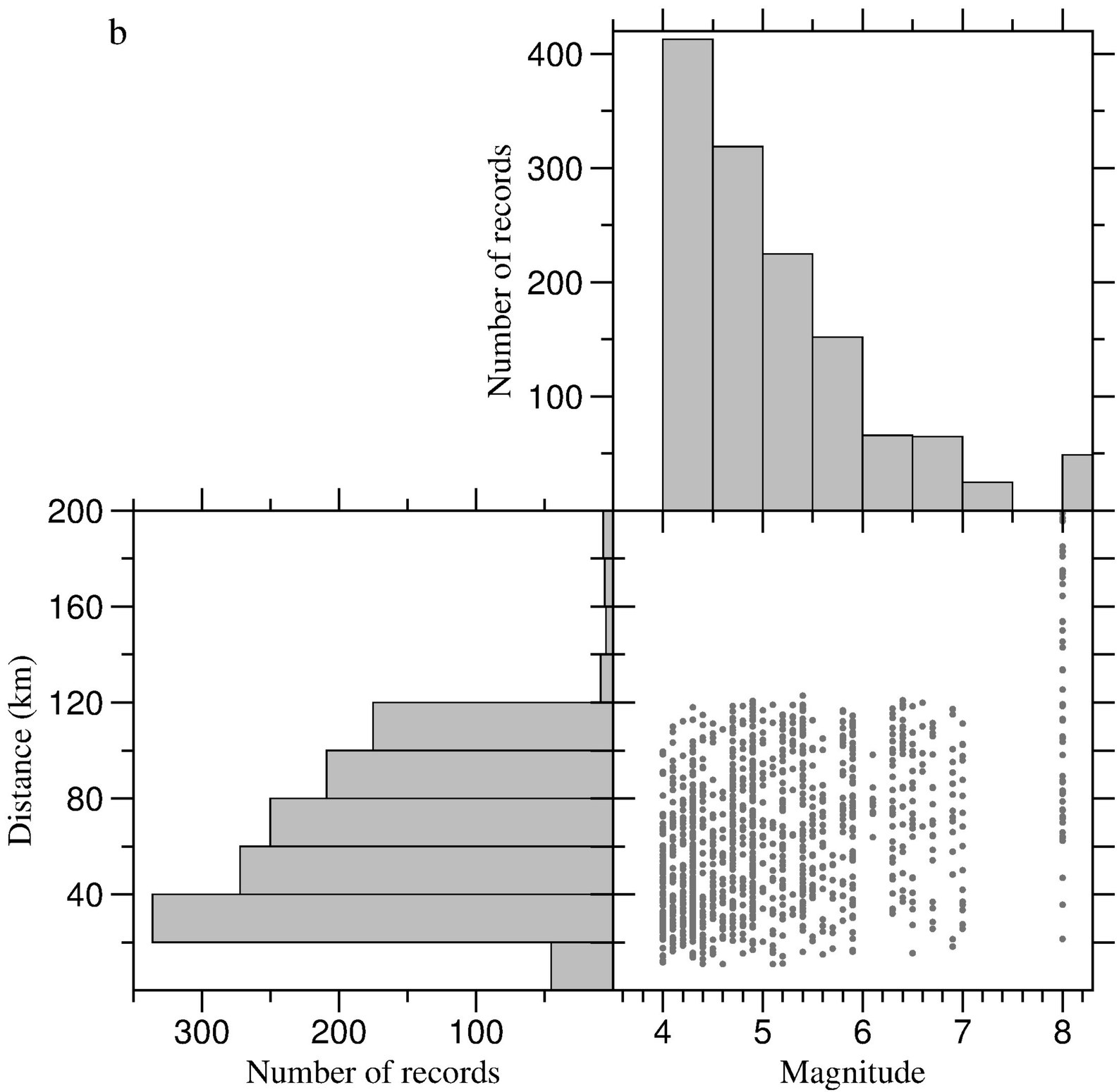
Number of records
Distance (km)
Magnitude
400
300
200
100
160
120
80
40
4
5
6
7
8

Figure 2.

M4.6

T_2

T_1

y_0

P_L

1.5
1.0
0.5
0.0
−0.5
−1.0
−1.5

0.0
0.1
0.2
0.3
0.4

LogPd(DistanceCorrected)

PwaveTimeWindow/(s)

Figure 3.

a

b

c

Magnitude Range: 4.0–8.0

Number of Events: 31

Distance Range: M≤7 R≤120km

M=8 R≤200km

Mag

LogPd(DistanceCorrected)

Compute Magnitude

$y_{model}-y_{obs}$

Pwave Time Window/(s)

Frenquency(%)

Figure 4.

LogPd(DistanceCorrected)

3.0
2.5
2.0
1.5
1.0
0.5
0.0
−0.5
−1.0
−1.5
−2.0

0 10 20 30 40 50 60 70 80 90 100 110 120 130

Pwave Time Window/(s)

Figure 5.

P_L^*

3
2
1
0
−1

P_L^*=0.763(0.068)M−3.291(0.374)

R^2=0.947 std.dev=0.170

4
5
6
7
8

CatalogMagnitude

Figure 6.

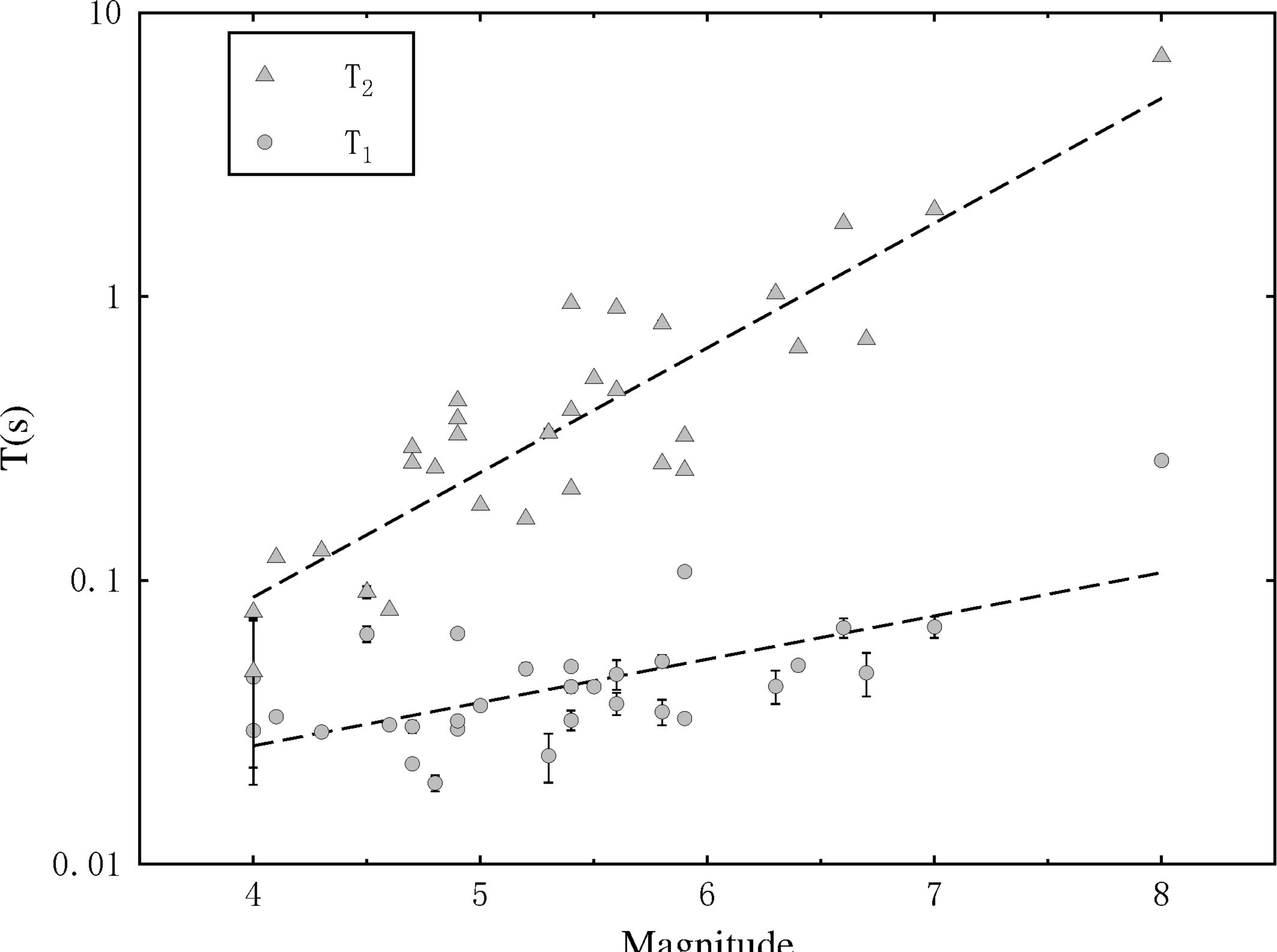
10
1
0. 1
0. 01
T(s)
4
5
6
7
8
Magnitude
T2
T1

Figure 7.

M>5.5

M≤5.5

Predicted Magnitude

Catalog Magnitude

4

5

6

7

8

9

Figure 8.

Vr=0.7Vs σ=0.1Mpa

a.

T_{PL}

T_{PL}

M=5.5
M=5
M=4.5
Fit Model

SHF(10^{16}Nm/s)

LSHF

T_2

T_2

Time/(s)

b.

$\log_{10}(T_{PL})=1.169*\log_{10}(T_2)+0.535$

$\mathrm{Log}T_{PL}$

$\mathrm{Log}T_2$

Figure 9.

Δσ=0.35Mpa
Δσ=0.1Mpa
Δσ=10Mpa
100
10
1
Source Radius(km)
10
1
0.1
Half Duration(T_{PL})
4
5
6
7
8
Magnitude

Figure 10.

T_{PL}

M(t) (10^{19} Nm/s)

0
1
2
3

0
20
40
60
80
100
120
140
160
180

Time/(s)

Figure 11.

Rupture length(km)

100

10

1

4

5

6

7

8

Magnitude

Circular model

Haskell model

Zhang et al. 2014(a)

Zhang et al. 2014(b)

Cheng et al. 2019

Wells Coppersmith

Figure 12.

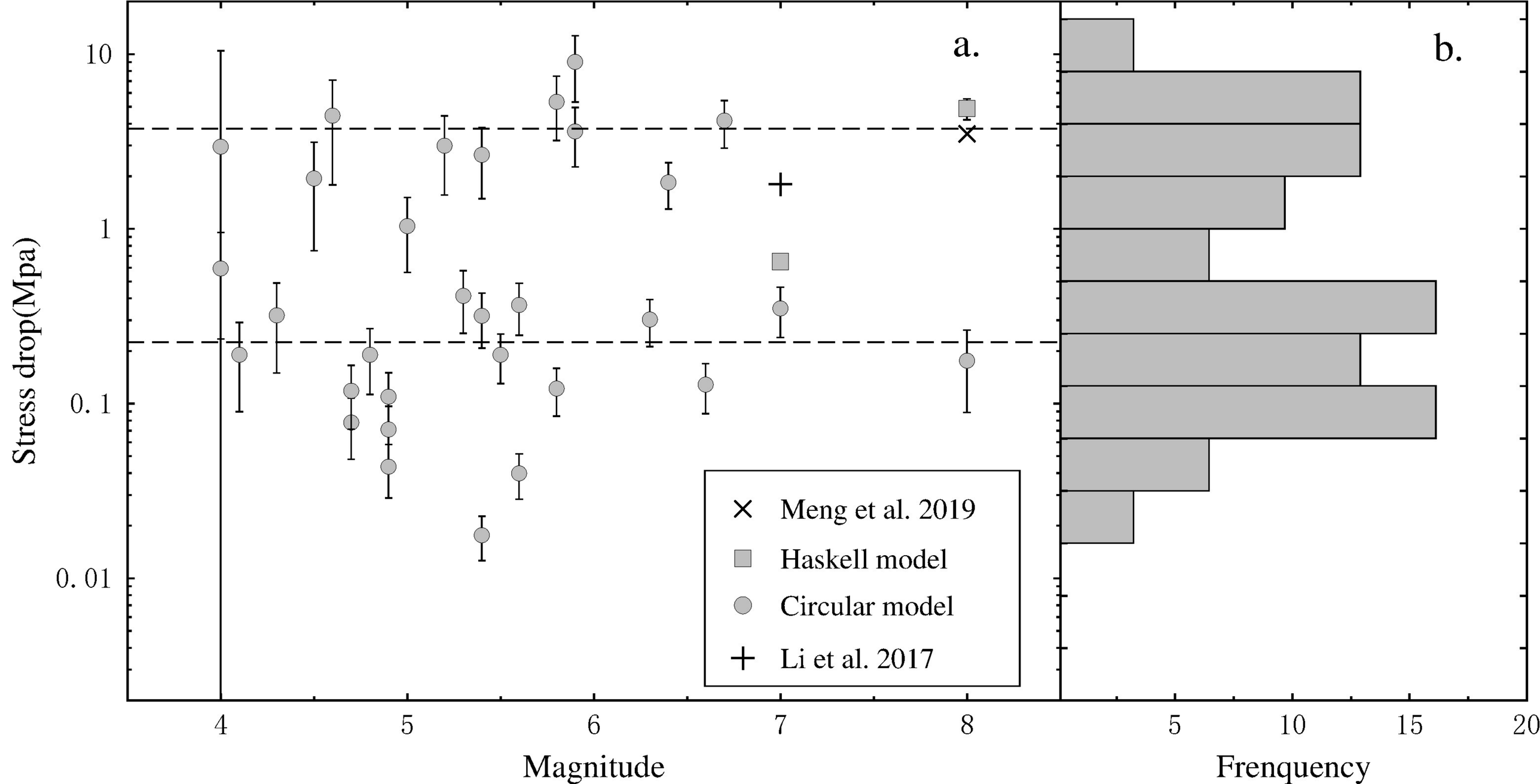
a.
b.
10
1
0. 1
0. 01
Stress drop(Mpa)
4
5
6
7
8
Magnitude
5
10
15
20
Frenquency
Meng et al. 2019
Haskell model
Circular model
Li et al. 2017

Figure S1.

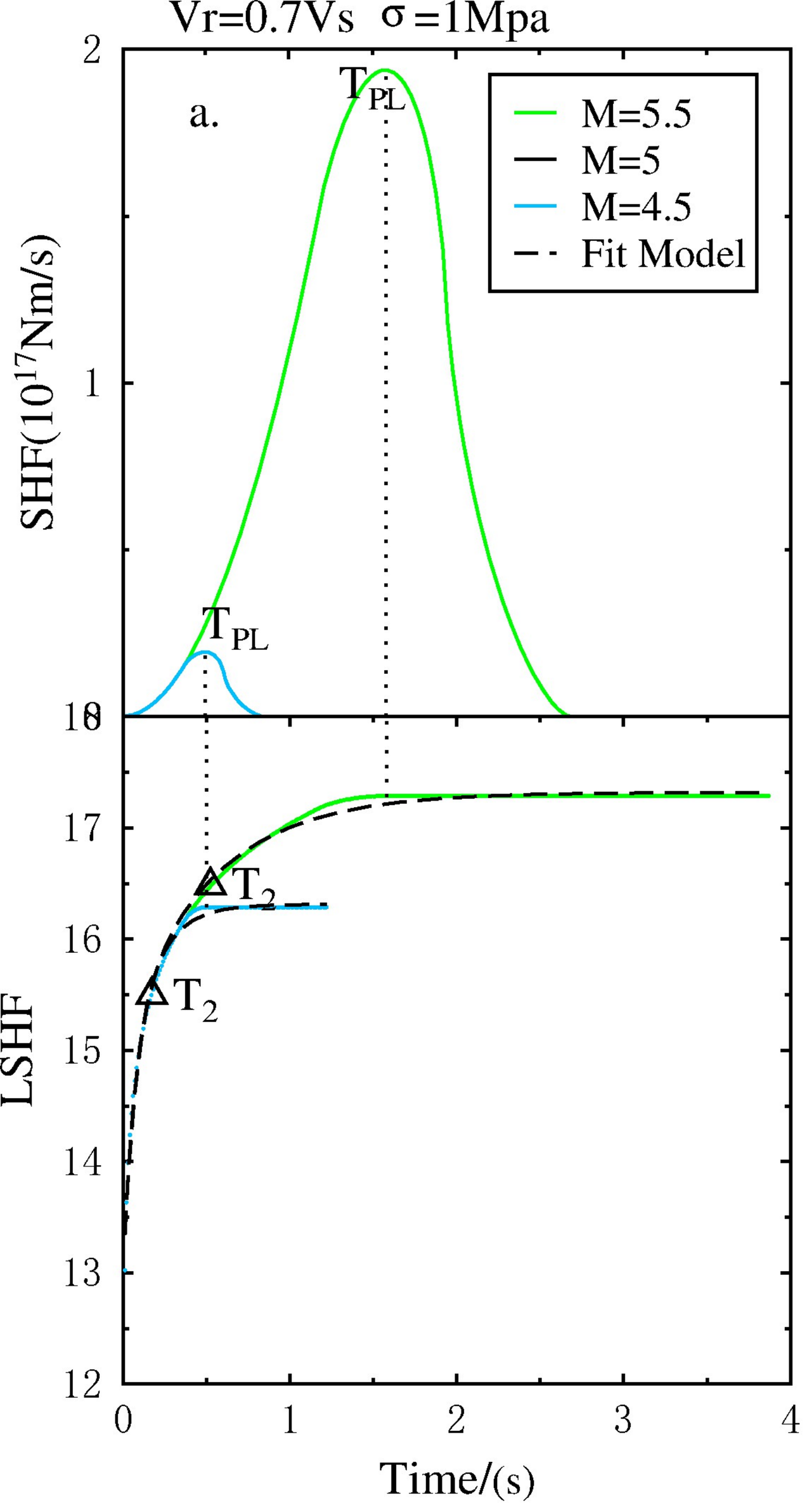
Vr=0.7Vs σ=1Mpa
a.
M=5.5
M=5
M=4.5
Fit Model
SHF(10^17Nm/s)
LSHF
Time/(s)

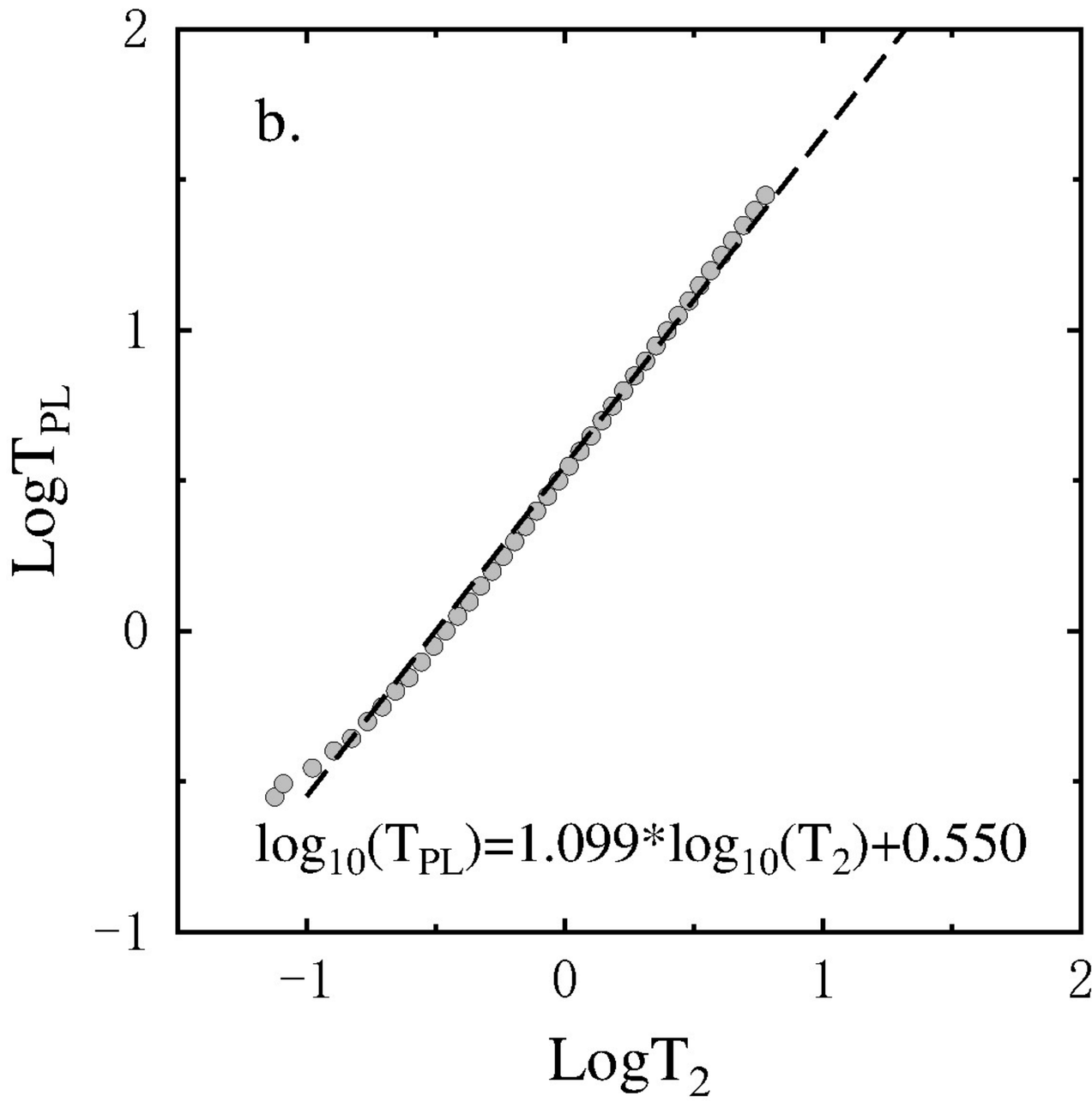
b.
LogT_PL
LogT_2
log10(T_PL)=1.099*log10(T_2)+0.550

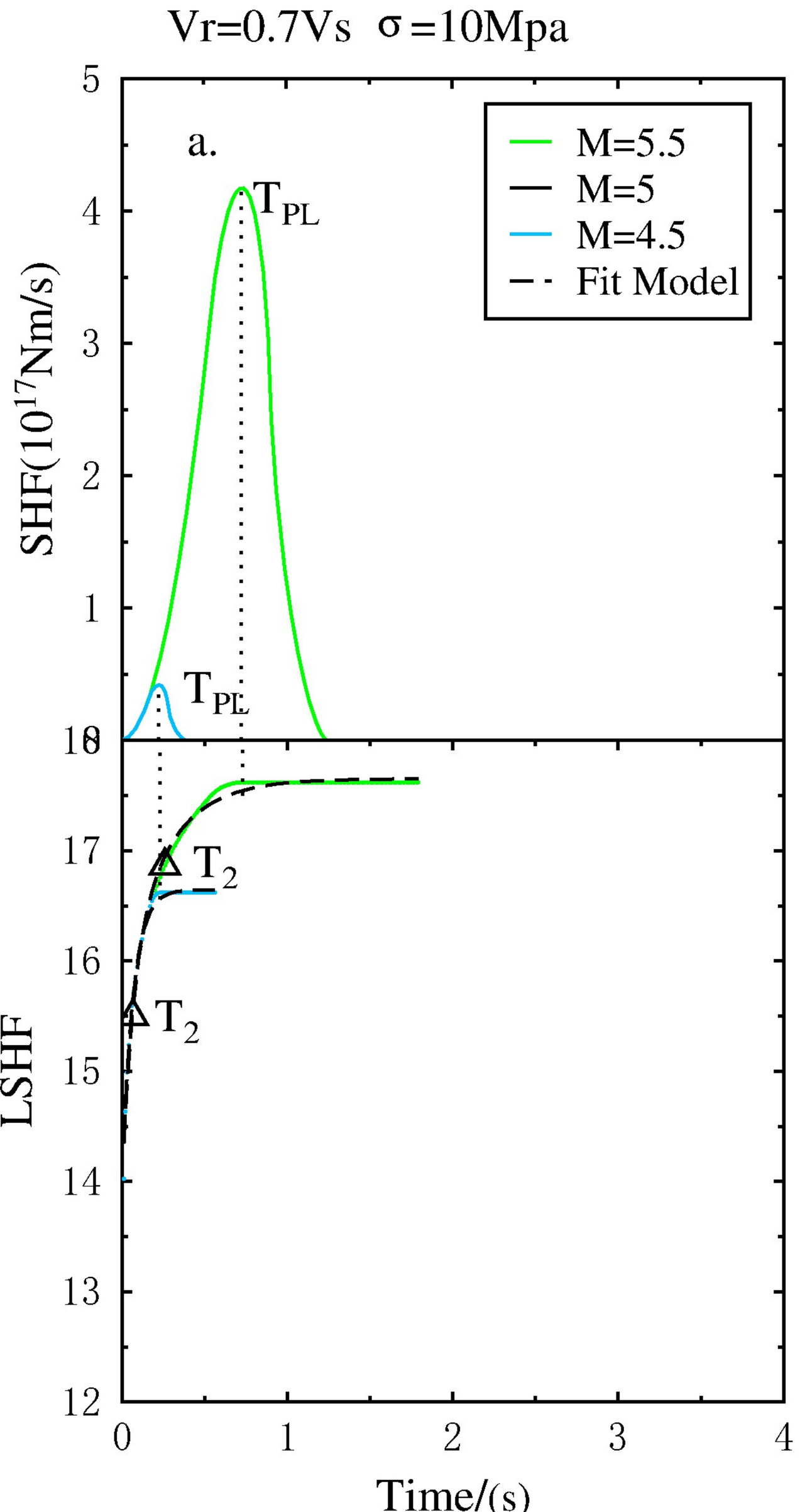
Vr=0.7Vs σ=10Mpa
a.
M=5.5
M=5
M=4.5
Fit Model
SHF(10^17Nm/s)
LSHF
Time/(s)

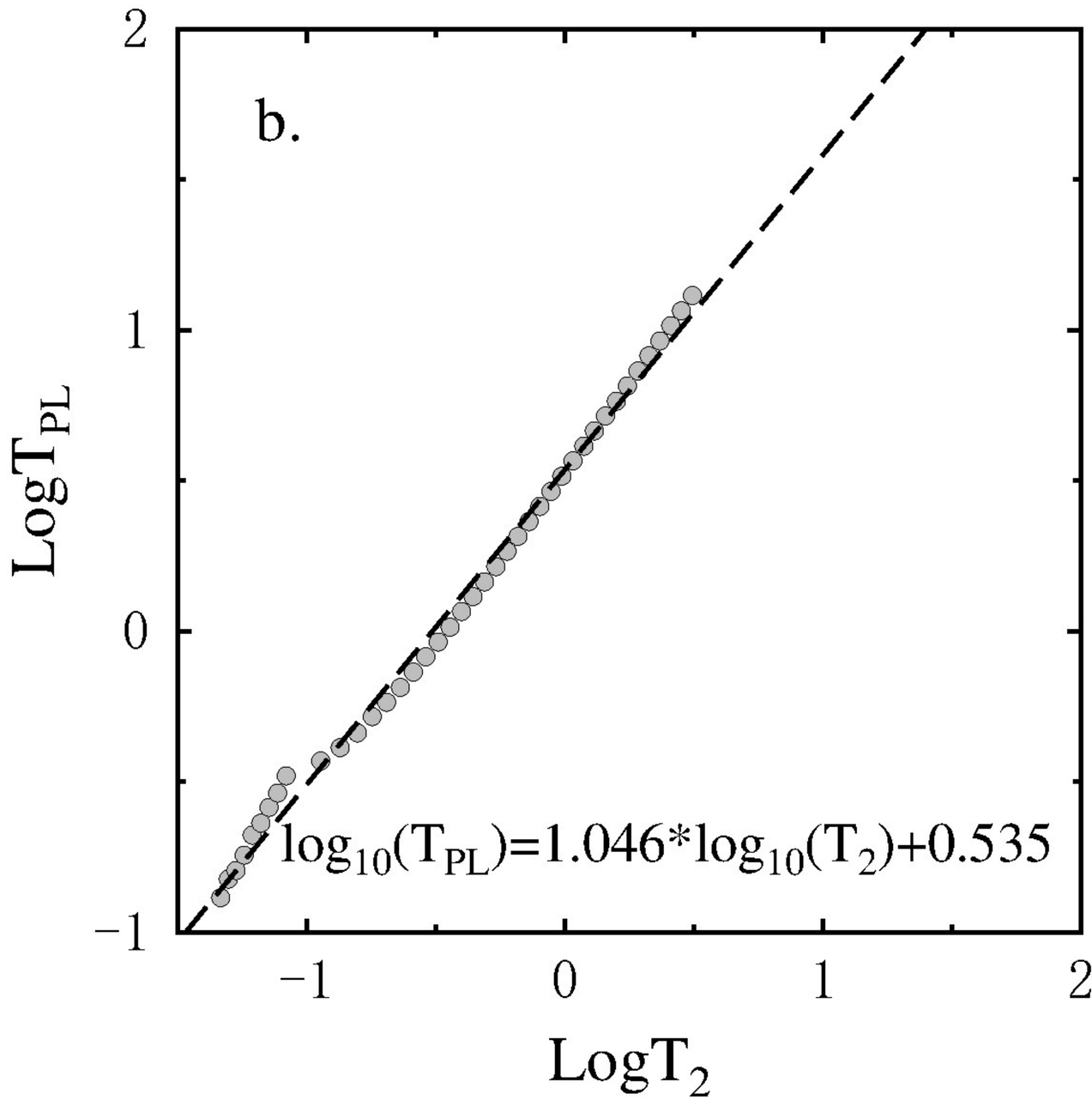
b.
LogT_PL
LogT_2
log10(T_PL)=1.046*log10(T_2)+0.535

No.	Location	Date	Epicenter		Magnitude			Half duration		Rupture parameters			Reference
			Lat.	Long.	M_S	M_S^{PRED}	M_W (source)	LPDT	GCMT	*SR (km)*	*RL (km)*	*SSD (Mpa)*	
1	Wenchuan	2008/05/12	31.00	103.40	8.0	8.3	7.9 (GCMT)	30.4	21.8	135.5	271 (circular)	0.18	This study
											326 (Haskell)	4.8	
											300		Zhang, Wang, Zschau, et al. (2014)
												3.5	Meng et al., 2019
2	Wenchuan (aftershock)	2008/05/13	31.43	104.06	5.8	5.9	5.6 (GCMT)	0.77	1.6	3.4	6.8	5.34	This study
										4.3		0.73	Wang et al. (2017)
3	Wenchuan (aftershock)	2008/05/14	31.34	103.63	5.8	5.7	5.4 (GCMT)	2.7	1.3	12.2	24.4	0.12	This study
										7.5		0.17	Wang et al. (2017)
4	Yaoan	2009/07/09	25.60	101.03	6.3	5.7	5.7 (GCMT)	3.6	1.8	16.0	32	0.30	This study
											15		Wang et al. (2011)
5	Fengnan	2010/04/09	39.59	118.11	4.1	4.1		0.3		1.5	3.0	0.19	This study
6	Qingchuan	2011/11/01	32.60	105.30	5.2	4.8	5.0 (GCMT)	0.47	0.8	2.1	4.2	3.00	This study
										2.3		1.29	Wang et al. (2017)
7	Tangshan	2012/05/28	39.71	118.47	4.7	4.7	4.7 (GCMT)	0.9	0.6	4.0	8.0	0.08	This study
8	Baodi	2012/06/18	39.61	117.56	4.0	3.3		0.1		0.5	1.0	2.95	This study
9	Baoying	2012/07/20	33.04	119.57	4.9	4.9	5.0 (GCMT)	1.0	0.8	4.5	9.0	0.11	This study
10	Yiliang	2012/09/07	27.56	104.03	5.6	5.6	5.3 (GCMT)	3.1	1.1	14.0	28	0.04	This study
11	Yongning	2012/11/20	38.43	106.34	4.6	4.6		0.2		0.9	1.8	4.44	This study
12	Eryuan	2013/03/03	25.93	99.72	5.5	5.5	5.4 (GCMT)	1.7	1.2	7.4	14.8	0.19	This study
13	Changji	2013/03/29	43.40	86.80	5.6	5.4	5.4 (GCMT)	1.5	1.3	6.7	13.4	0.37	This study
14	Lushan	2013/04/20	30.30	103.00	7	7.0	6.6 (GCMT)	7.6	4.9	34	68	0.35	This study
											77.3 (Haskell)	0.65	
											60		Zhang, Wang, Chen, et al. (2014)
												1.8	Li et al., (2017)
15	Lushan (aftershock)	2013/04/20	30.28	102.93	4.8	4.2		0.7		3.3	6.6	0.19	This study
16	Lushan (aftershock)	2013/04/20	30.25	102.83	4.7	4.6		0.8		3.5	7	0.12	This study
17	Lushan (aftershock)	2013/04/20	30.28	102.99	4.9	4.7		1.2		5.2	10.4	0.07	This study
18	Lushan (aftershock)	2013/04/20	30.33	102.92	4.3	4.0		0.4		1.6	3.2	0.32	This study
19	Lushan (aftershock)	2013/04/20	30.24	102.94	5.4	5.4	5.4 (GCMT)	3.3	1.2	14.6	29.2	0.02	This study
20	Lushan (aftershock)	2013/04/20	30.31	103.04	4.0	3.6		0.2		0.9	1.8	0.59	This study
21	Lushan (aftershock)	2013/04/21	30.36	103.05	5.4	4.8	4.8 (GCMT)	0.6	0.6	2.7	5.4	2.65	This study
22	Lushan (aftershock)	2013/04/21	30.26	103.00	4.9	4.6	5.0 (GCMT)	1.4	0.8	6.1	12.2	0.04	This study
23	Lushan (aftershock)	2013/04/21	30.34	103.00	5.4	5.1	5.2 (GCMT)	1.2	0.9	5.6	11.2	0.32	This study
24	Minxian	2013/07/22	34.54	104.21	6.7	6.6	6.0 (GCMT)	2.4	2.4	10.6	21.2	4.16	This study
											11		Sun et al., 2015
											10		Wang et al., 2014c
25	Menyuan	2013/09/20	37.73	101.53	5.3	5.1	5.1 (GCMT)	1.0	0.8	4.5	9	0.41	This study
26	Ludian	2014/08/03	27.11	103.33	6.6	6.5	6.2 (GCMT)	6.7	2.9	30.0	60	0.13	This study
											12		Cheng et al., 2015; Wang et al., 2014d
27	Kangding	2014/11/22	30.29	101.68	6.4	6.2	6.1	2.2	2.8	9.8	19.6	1.85	This study

							(GCMT)				20		Fang et al., 2015b
											16		Jiang et al., 2015
											12		Yi et al., 2015
28	Kangding	2014/11/25	30.20	101.75	5.9	5.6	5.7 (GCMT)	0.7	1.8	3.2	6.4	9.02	This study
29	Jinggu	2014/12/06	23.32	100.50	5.9	6.0	5.5 (GCMT)	1.0	1.5	4.4	8.8	3.61	This study
30	Leshan	2015/01/14	29.30	103.20	5.0	4.8	4.9 (GCMT)	0.5	0.7	2.4	4.8	1.03	This study
31	Songming	2015/03/09	25.33	103.10	4.5	4.9	4.8 (GCMT)	0.2	0.6	1.1	2.2	1.94	This study
MSPRED = Predicted Ms, SR = source radius, RL = rupture length =2*source radius, SSD = statics stress drop, GCMT data are available at www.globalcmt.org (last accessed May.6, 2020)													

1